Full Length Article

Understanding crystallization in undoped and nitrogen doped GeTe thin films using substrate curvature measurements

Piyush Jagtap [a,d,1,*], Christophe Guichet [a], Raj Tholapi [a], Pierre Noe [b], Cristian Mocuta [c], Olivier Thomas [a]

[a] IM2NP CNRS UMR 7334, Campus de St-Jérôme, Aix-Marseille Université, Cedex 20, Marseille 13397 France
[b] Université Grenoble Alpes, CEA, LETI, 17 rue des Martyrs, Grenoble 38054, France
[c] l'Orme des Merisiers, Synchrotron SOLEIL, Saint-Aubin BP 48, Gif-sur-Yvette 91192, France
[d] Materials science and Metallurgical Engineering, Indian Institute of Technology, Kandi, Hyderabad, Sangareddy 502285 India

ABSTRACT

Herein, we study the crystallization of undoped and nitrogen doped amorphous GeTe thin films (slightly rich in Ge) obtained by sputtering using substrate curvature measurements to understand the underlying mechanisms controlling stress evolution in the film throughout the phase transformation. At temperatures below crystallization temperature, amorphous films showed stress relaxation and the stress gradually became tensile with annealing time. The GeTe samples show a two-step crystallization wherein amorphous GeTe crystallized first (at the crystallization temperature T_x) followed by crystallization of excess Ge (Ge precipitation) at -T_x+50 °C. Upon GeTe crystallization, a sharp increase in the tensile stress is explained using a coalescence mechanism. This interpretation resolves the issue of the discrepancy between the measured stress buildup reported by several authors and the predicted stress jump from elastic accommodation of density change. The precipitation of excess Ge (from amorphous to crystalline) along grain boundaries in GeTe leads to compressive stress build-up. Nitrogen doping affects both the GeTe and Ge crystallization events leading to lesser tensile and compressive stress. The models for stress relaxation in the amorphous phase, stress build-up due to GeTe, and excess Ge crystallization are discussed.

1. Introduction

The ability to reversibly switch between the amorphous and crystalline phases in chalcogenide phase-change materials (PCM) has recently attracted a lot of attention. The most commonly studied phase-change alloys are the ternary compound belonging to the GeTe-Sb$_2$Te$_3$ pseudo-binary line of the Ge-Sb-Te phase diagram such as GeTe and Ge$_2$Sb$_2$Te$_5$ (GST) among the broad class of PCMs [1,2]. Particularly, GeTe is the simplest binary alloy that has been extensively studied for non-volatile memory applications. A drastic difference in the physical, electrical, as well as optical properties between the amorphous and crystalline state of phase-change materials, and a rapid [3,4] and reversible transformation between the two phases [5] make them ideal for phase-change random access memory (PCRAM) [2,6] and optical memory storage such as CD-RW and DVD-RAM [7]. In PCRAM memory devices, phase-change material in form of a thin film of a patterned cell is sandwiched between two metallic electrodes. The transformation from amorphous to crystalline phase is achieved by applying electrical pulses [8]. The data can be stored and read in two distinct resistance states owing to the large resistivity contrast (-10^3–10^6 Ohm.cm depending on GeTe-Sb$_2$Te$_3$ alloy composition) between the amorphous and crystalline phases of the PCM.

Although PCM alloys have promising properties, multiple challenges have limited their large-scale integration [2]. PCM alloys show a large change in density when they undergo crystallization from the amorphous phase [2,9]. Several authors argued that density change during crystallization is accompanied by excessive stress build-up in the films that can cause extensive cracking of the film [10]. This presents a serious reliability and durability concern in the phase-change devices after multiple cycles [11]. Therefore, understanding the stress and the ability to control it is crucial for successful device integration. The stability of the amorphous phase and data retention time is another important issue

---

in the reliability of PCM memory devices [8]. The resistivity measurements showed a continuous drift in the resistivity of the amorphous films during aging or annealing (commonly known as the "resistance drift" phenomenon). The exact mechanism underlying this phenomenon is under constant debate [12] and it is usually attributed to the structural relaxation of the as-deposited or melt-quenched amorphous phase [13, 14]. The increase or decrease of disorder or defect concentrations [15–20], increase [21] or decrease [22] in Ge-Ge homopolar bonds are some of the phenomena that have been suggested as being responsible for the resistance drift. Ge enrichment or doping with small amounts of carbon or nitrogen allows stabilization of the amorphous phase and shows better data retention in memory devices [8]. However, it is not clear how Ge enrichment or doping affects the structural relaxation and stress build-up during crystallization. Additionally, segregation and precipitation of Ge in highly Ge-enriched off stoichiometric alloys were found to cause premature failure in the PCRAM devices [23]. Furthermore, doping of GeTe films with small quantities of C, N, or O changes their crystallization temperature and overall density change upon crystallization. The controlling doping amount was proposed to develop zero volume change PCMs to minimize the stresses in the films [10, 24–26]. The crystallization temperature increases with increasing the heating rate because it is a thermally activated process that may be characterized by activation energy [27]. Therefore, a detailed understanding of thermo-mechanical behavior during reversible phase transformation of these slightly off stoichiometric and doped alloys is essential.

Most of the previous works on PCM alloys employed optical reflectance or four-point probe sheet resistance measurement [28–31] techniques to study the amorphous to crystalline transformation in these alloys. Although such studies have proved extremely useful in understanding the kinetics of transformation, they do not provide much insight into structural changes occurring during the transformation. Therefore, such measurements were often supplemented by X-ray diffraction (XRD) [32,33] and extended X-ray absorption fine structure (EXAFS) measurements [34] to reveal the structural changes at the atomic level. The previous studies using molecular dynamics (MD) simulations supported by Raman spectroscopy have shown that the amorphous GeTe contains a mix of tetrahedral and defective octahedral coordination of atoms [22,35–38]. Furthermore, switching from tetrahedral and defective octahedral environments to octahedral coordination of atoms occurs upon crystallization [22,39,40]. However, such studies do not correlate structural changes with stress evolution in films.

The substrate curvature measurement is a useful technique that correlates real-time curvature measurements to the change in the internal stress of the film [41]. Such studies have proved extremely useful in understanding the mechanisms that govern the residual stress evolution in thin films during growth [41] but are rarely used to understand phase transformation in phase-change materials [32,33,42–44]. The earliest study by Pedersen et al. [43] showed a sharp increase in the tensile stress at the crystallization temperature of various PCM alloys. Yahia et al. [42] showed crystallization temperature increased with decreasing the thickness of the GeTe films and crystallization temperature remained unchanged by the thermal history of the amorphous phase. More recently, Gallard et al. [33] used combined curvature and *in-situ* X-ray diffraction and showed that GeTe crystallization occurred in two steps wherein GeTe crystallized first followed by crystallization of excess Ge. A sudden rise in tensile stress was observed upon GeTe crystallization. At slightly higher temperatures, excess Ge in the film crystallized and an abrupt increase in compressive stress was observed at the same temperature [33]. Although a sudden increase followed by a decrease in stress was correctly correlated with the GeTe and Ge crystallization events, the prediction of stress during such events remained challenging. The modeling of stress evolution throughout the transformation will be useful to predict the stress relaxation in the amorphous phase and stress build-up during the crystallization events. According to existing literature, the stress induced during crystallization of GeTe is so

far explained purely in terms of volumetric strain between amorphous and crystalline phase. However, the stress predictions based on such simplistic model are unrealistic and orders of magnitude off from the experimentally measured values. The discrepancy was explained by concurrent stress relaxation mechanisms during crystallization [33,42, 43]. In this work, we suggest an alternative mechanism based on the crystallite coalescence, akin to operating during the thin film growth when nucleated islands on the substrate begin to coalesce thereby inducing a tensile stress. The predictions based on our model are consistent with the experimental values. We believe this model can be generalized for prediction of crystallization induced stress in other materials systems undergoing amorphous to crystalline phase transformation.

Accordingly, in this paper, we report real-time curvature measurements on slightly off-stoichiometric, undoped GeTe, and 5–10% nitrogen-doped GeTe thin films during *in-situ* annealing. The isothermal annealing at various temperatures along with real-time curvature measurements were performed to understand stress relaxation and/or stress build-up in the amorphous and crystalline phases. The curvature measurements were complemented with scanning electron microscopy (SEM), transmission electron microscopy (TEM), and synchrotron X-ray diffraction to correlate stress with microstructural changes that occur during the crystallization. The models for stress relaxation and stress build-up during the transformation are discussed.

2. Experimental procedure

100 nm GeTe films were deposited on 100 µm thick Si (100) wafers using magnetron sputtering of a pure GeTe target in a 200 mm industrial deposition tool. The composition of the films, as usual using the sputtering technique, was slightly enriched in Ge leading to compositions close to $Ge_{53}Te_{47}$ in the deposited films as revealed by Wavelength Dispersive X-ray Fluorescence (WDXRF) measurements [45]. Nitrogen-doped (5–10%) GeTeN samples were also fabricated using reactive magnetron sputtering with controlled Ar/N_2 gas amounts introduced in the sputtering plasma. The deposited GeTe films were capped with an additional 10 nm SiO_2 layer without breaking vacuum to prevent surface oxidation. The microstructure of all the samples fabricated by sputtering was amorphous in the as-deposited state.

The curvature of the samples was measured in real-time using a laser curvature system (*K-space associates, USA*) while the samples were heated using a hot stage inside a vacuum chamber. A constant heating rate of 2 °C/min, or 10 °C/min was used in the experiments. The temperature was recorded on a reference Si piece fixed on the heating stage using a K-type thermocouple. The background pressure during all the curvature measurements was 10^{-6} mbar or better. An *in-situ* spectroscopic ellipsometry measurement was performed on similar 100 nm GeTe samples under N_2 atmosphere. The crystallization temperature, T_x around 230 °C was found for rhombohedral GeTe phases using a heating ramp rate of 10 °C/min (see the Supplementary Material Fig. S**1**). These values are in good agreement with the expected crystallization temperature values for a non-oxidized GeTe film [32,33,42,44].

The stress in the films deposited on Si substrate coupons (2 cm x 2 cm) during temperature cycling was estimated using Stoney's formula that relates stress × thickness (force per unit width) with the measured curvature using the following formula:

$$\sigma_f h_f = \frac{1}{6} M_s h_s^2 \kappa \qquad (1)$$

where σ_f is the stress in the film, h_f is the film thickness, h_s is the thickness of the Si substrate (100 µm), M_s is the biaxial modulus of the substrate and κ is the measured curvature of the samples. The curvature measurements were performed relative to the substrate reference of as-deposited films. Therefore, although residual compressive stresses in the sputtered GeTe films are expected (Usually in the 50–100 MPa range

depending on film thickness), they were not considered in this study, and only variations compared to this initial state are thus reported. The curvature of bare Si piece without GeTe film during thermal cycling remained unchanged and hence measured curvature of GeTe films on Si substrate can be attributed to change in the stress in GeTe films.

In-situ crystallization of the GeTe thin films was also followed up using XRD at the SOLEIL Synchrotron facility (France). An Anton Paar® heating stage was used to anneal the samples under a nitrogen atmosphere, with typical heating and cooling rates set to 5 °C/min and 20 °C/min respectively. The furnace was mounted on the six-circle diffractometer (Kappa geometry) of the DiffAbs beamline at SOLEIL Synchrotron, and a typical beam size of -200 × 250 μm^2 (FWHM, vertical × horizontal) was used for the measurements. The XRD experiments were performed at a photon energy of 18 keV in vertical scattering geometry, with a fixed incident angle of 2° The data was recorded using a two-dimensional hybrid pixel array detector (XPAD) [46,47]. The diffracted intensities as a function of the scattering angles 2θ were obtained after applying geometrical corrections and background subtraction to the data, followed by 1D azimuthal integration [48,49]. More details about the setup and the experimental approach can be found in references [33,50].

The microstructure of the films at various stages during the transformation was characterized using SEM and TEM. Focused ion beam (FIB) milling and polishing was used to prepare a thin cross-section lamella for TEM characterization. Energy dispersive spectroscopy (EDS) was used for elemental analysis using TEM.

3. Results

The amorphous to crystalline phase transformation was achieved by heating to temperatures above the crystallization temperature (T_x) and cooling back to the room temperature (RT) (which we will address as the crystallization cycle) at a constant heating and cooling rate. The reverse transformation can be achieved by heating above the melting point (T_m) followed by ultrafast cooling by quenching from the liquid state (amorphization cycle). However, such ultrafast cooling rates were inaccessible, and hence in the present work, we focus on the crystallization cycle only. The curvature of the samples was monitored during the crystallization cycle with a constant heating and cooling rate of 10 °C/min. Typical real-time stress evolution in 100 nm GeTe film deposited on Si substrate during the heating and cooling cycle is shown in Fig. 1.

In the initial stage of the heating cycle, as shown in Fig. 1, the amorphous GeTe films deposited on the Si substrate undergo thermoelastic compression due to the difference in the coefficient of thermal expansion (CTE) of amorphous GeTe film ($\alpha_{\text{a-GeTe}} = 4.8 \times 10^{-6}$ / °C^2) and Si substrate ($\alpha_{\text{Si}} = 3 \times 10^{-6}$ / °C). Above 140 °C, the curvature or stress×thickness spontaneously increased in the positive direction making film stress more tensile. At T_x a sharp jump in tensile stress was observed. With further heating (above T_x) the crystallized polycrystalline GeTe films briefly develop a steady linear compressive stress regime. This can be attributed to a CTE mismatch between crystalline GeTe film ($\alpha_{\text{c-GeTe}} = 12.42 \times 10^{-6}$ / °C^1) and Si substrate. Note that the crystalline GeTe film have a much higher thermal expansion coefficient compared to amorphous GeTe. This is consistent with the previous studies showing an abrupt change in the density, modulus as well as CTE upon GeTe crystallization [33,43,51]. At the crystallization temperature of the Ge, T_{Ge} (~T_x+50 °C), a sudden jump in the compressive direction was observed. This is shown using dotted lines in Fig. 1b, the slope of the dotted line became much steeper at T_{Ge}. The stress change due to excess Ge crystallization was estimated from the intersection point of these

dotted lines where the slope abruptly changes. Our previous work using combined curvature and *in-situ* diffraction experiments correlated the sharp jumps in tensile and compressive direction to the GeTe crystallization and excess Ge crystallization, respectively [33].

To further understand the details of underlying processes occurring at different stages during the transformation, curvature measurements during isothermal annealing at various temperatures (80, 100, and 120 °C) were performed. The samples annealed under isothermal conditions below 140 °C showed stress relaxation by the viscous flow process in the amorphous phase. The stress relaxation in 100 nm undoped GeTe, as well as 5–10% nitrogen-doped GeTe films, is shown in Fig. 2. The relaxation in the amorphous phase of all the samples occurred in the tensile direction. The relaxation occurred more rapidly with a small increase in temperature from 80 to 120 °C. A comparison of the relaxation behavior of undoped (Fig. 2b) and nitrogen-doped GeTe samples (Fig. 2c,d) showed nitrogen doping slows down the kinetics of stress relaxation in amorphous GeTe. This relaxation in amorphous phase is also called as structural relaxation, wherein atoms rearrange to minimise the energy.

It is important to highlight here that absolute stress should relax to a stress-free state at the end of isothermal relaxation. However, we only measure relative stress as the initial residual compressive stress in the films was unknown. Therefore, all stress curves start from an arbitrary initial value of zero stress. Nevertheless, due to rapid stress relaxation in the amorphous phase before crystallization temperature, the stress at the onset of crystallization is expected to be low. Therefore, initial residual stress is not expected to affect the crystallization behavior of GeTe films significantly. This is further justified by the comparison of crystallization behavior of the pre-annealed and as-deposited GeTe films wherein, different initial stress levels do not seem to affect the kinetics as well as the magnitude of the stress build-up during GeTe crystallization substantially (Fig. 3).

The same set of samples used in isothermal annealing experiments (pre-annealed) were subjected to a crystallization cycle to understand the effect of pre-annealing (thermal history) on the crystallization behavior. A comparison of the crystallization cycle of as-deposited and the isothermally annealed (for 12 h at various temperatures) is shown in Fig. 3. The pre-annealed samples have a higher value of initial tensile stress due to partial stress relaxation during isothermal pre-annealing and subsequent tensile stressing during the cooling segment. Therefore, the transition from negative to positive curvature occurred at higher temperatures and higher stress, compared to as-deposited thin film samples. The structural relaxation regime (period of steady positive curvature change) progressively reduced with the annealing temperature as compared to the total relaxation observed in the unannealed (i.e., as-deposited) films (shown with vertical lines in Fig. 3). This observation indicates that the structural relaxation (leading to re-arrangement of atoms) of the amorphous films during isothermal annealing was irreversible. Interestingly, and consistent with previously reported results [42], the crystallization temperature remained almost unchanged by the prior thermal history of the samples. Further experiments are needed to examine the differences in the activation energy of crystallization and incubation time between pre-annealed and as-deposited samples.

The microstructure of the films at various stages during the phase transformation was observed using SEM and is shown in Fig. 4. The as-deposited film surface was featureless. After annealing, dark circular features appeared on the free surface (identified as blisters in SiO$_2$ capping layer, see Supplementary Material Fig. S3). The rest of the film showed no contrast as the film was still amorphous. When heated above T_x, (Fig. 4c) GeTe grains surrounded by a thin dark shell was visible in the SEM micrographs (network of dark contrast along grain boundaries, see inset of Fig. 4c). This dark contour arises from the segregation of amorphous Ge whereas GeTe appears bright due to the difference in the atomic contrast. This contrast disappears when switched to secondary electron mode and hence must arise from phase contrast between crystalline GeTe and excess Ge (See Fig. S2 in Supplementary Material).

---

[2] The coefficient of thermal expansion of amorphous and crystallized GeTe films was determined using double substrate curvature measurements. GeTe films of same thicknesses were deposited on 100 μm thick glass substrate.
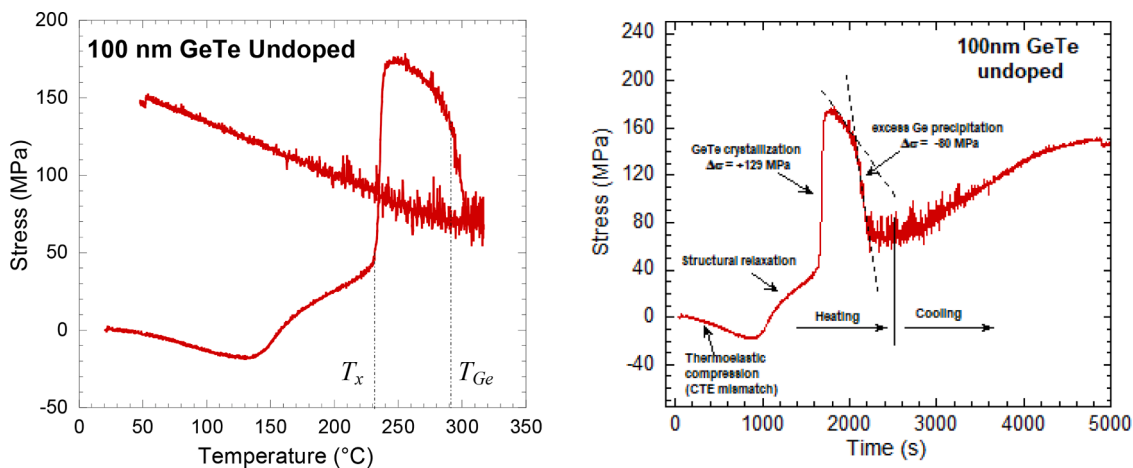
Fig. 1. The relative variation in stress, monitored by curvature changes in the 100 nm undoped GeTe thin film during heating (up to 320 °C) and cooling back to RT shown as a function of (a) temperature and (b) time. The measurements were performed under a vacuum (10^{-6} mbar) with a constant heating and cooling rate of 10 °C/min.
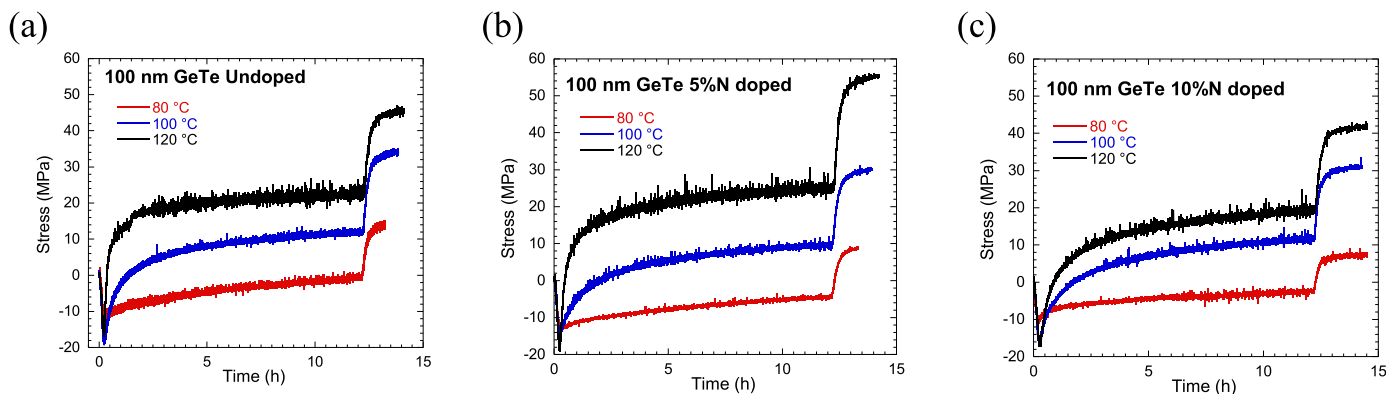

Fig. 2. The stress relaxation in amorphous GeTe films under isothermal annealing conditions. Stress evolution in: (a) undoped GeTe, (b) 5% nitrogen-doped and (c) 10% nitrogen-doped GeTe films are shown. The initial linear segment corresponds to a heating ramp followed by 12 h of isothermal annealing during which stress relaxation was observed. The final segment with sudden tensile stress evolution corresponds to cooling to RT.
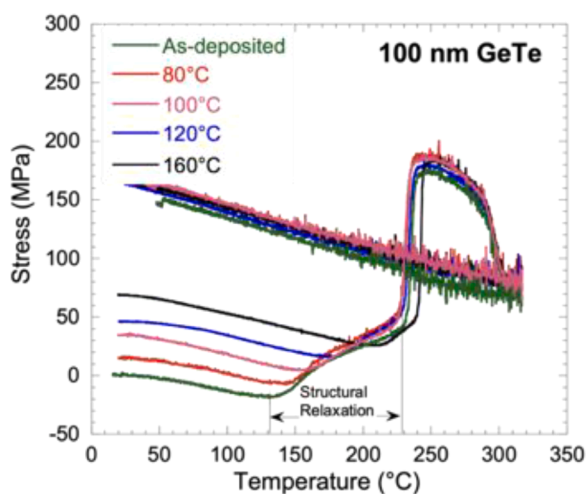

Fig. 3. The stress change in the as-deposited and pre-annealed (12 h) 100 nm GeTe thin films during the crystallization cycle. The region where curvature steadily increases in the positive direction due to structural relaxation is highlighted using vertical lines and arrows for as-deposited samples.

Such elemental segregation along grain boundaries or surfaces was also observed in previous works in other PCM alloys such as GST [51–53].

Consistent with our previous work [33], XRD measurements confirmed crystallization of the rhombohedral GeTe phase, but no diffraction peak corresponding to crystalline Ge was observed at T_x, confirming that excess segregated Ge was still amorphous. The 111 reflection of cubic Ge was detected (using XRD) in samples heated to temperature T_{Ge} and above (see Fig. 6a). Interestingly, the comparison of SEM images before and after the excess Ge crystallization indicates that Ge crystallized mostly at the GeTe grain boundaries in form of grain boundary precipitate (see insets of Fig. 4c and d). The SEM (taken at a tilt angle of 45°) and FIB cross-section micrographs showed that the dark circular features observed on the sample surface originated from the blisters in the SiO_2 capping layer (see Supplementary material Fig. S3). The blisters were also noticed in the uncrystallized films after thermal annealing, see Fig. 4b. Therefore, volume change upon crystallization is not the cause for the formation of blisters. Such blisters may result from compressive stress induced in the SiO_2 layer during cooling due to CTE mismatch between SiO_2 and Si substrate. Note that the CTE of SiO_2 is lower than the Si, therefore, heating and cooling will induce tensile and compressive stress in the SiO_2 capping layer, respectively. However, since the thickness of SiO_2 capping layer is only 10 nm its contribution to the overall measured stress in GeTe films can be neglected. It is important to point out that Ge segregation is not responsible for the dark appearance of the blisters. Blisters appear dark in-lens mode due to their hollow

(a)

(b)

(c)

(d)
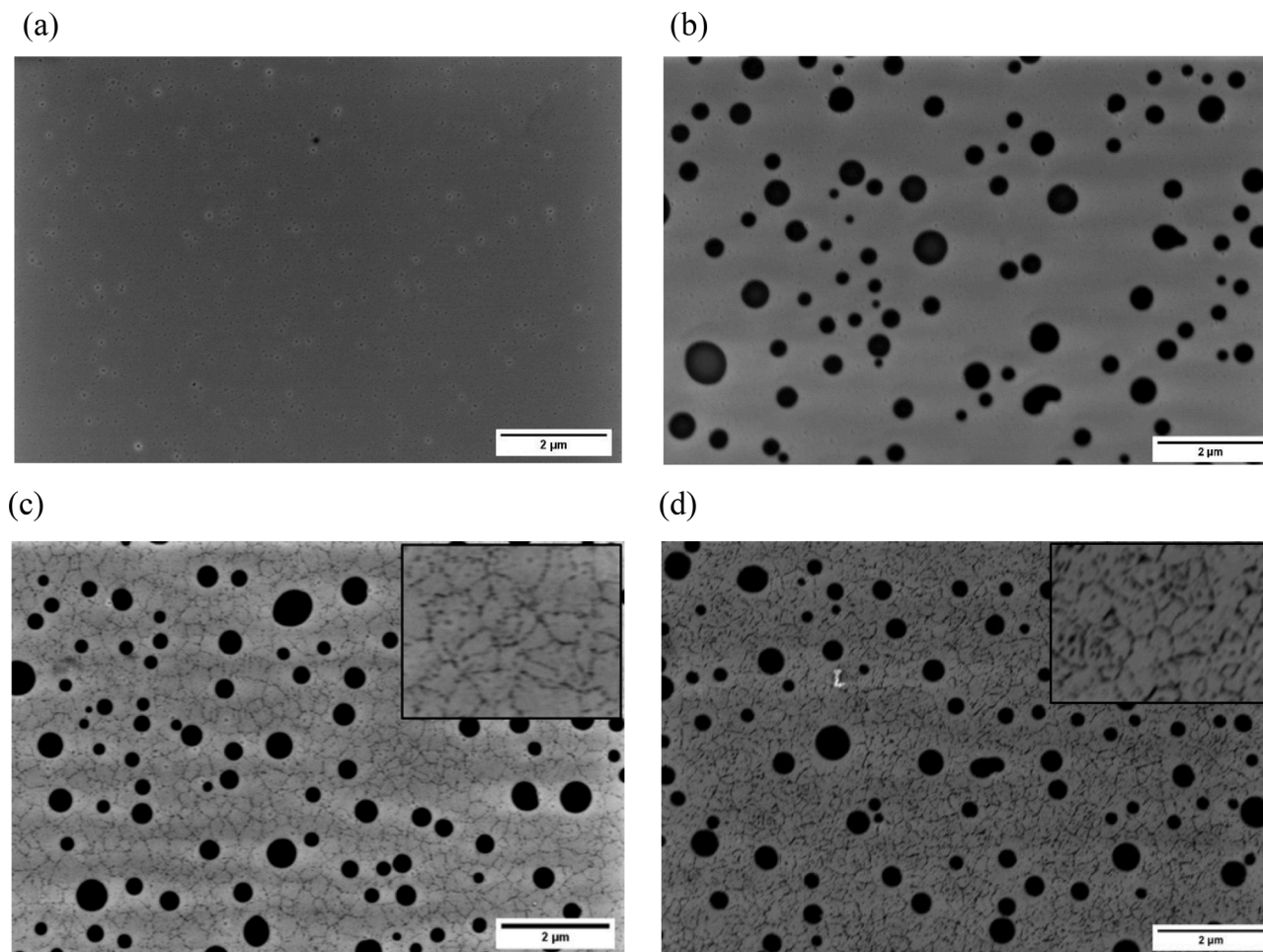
Fig. 4. The plan-view scanning electron micrographs (with in-lens detector) of the 100 nm GeTe thin films at various stages during the amorphous to crystalline transformation: (a) as-deposited, (b) annealed at 220 °C and cooled back to RT (still amorphous), (c) annealed to a temperature of 290 °C, higher than T_x of GeTe and cooled to RT (GeTe is crystallized, excess Ge amorphous), and (d) annealed at temperatures of 400 °C higher than T_{Ge} and cooled to RT (both GeTe and excess Ge are crystallized).

structure. The contrast completely turns off when a low voltage electron beam (0.5–1 kV) was used or in SE mode (See Fig. S2 in Supplementary Material)

The SEM images in Fig. 5 show the top surface of the nitrogen-doped films. A couple of interesting observations can be made from Fig. 5. Compared to the undoped samples (Fig. 4d) 5% N-doped samples showed reduced segregation of of excess Ge at the grain boundaries (Fig. 5a). In the GeTe films with 10% nitrogen, excess Ge segregation at

(a)

(b)
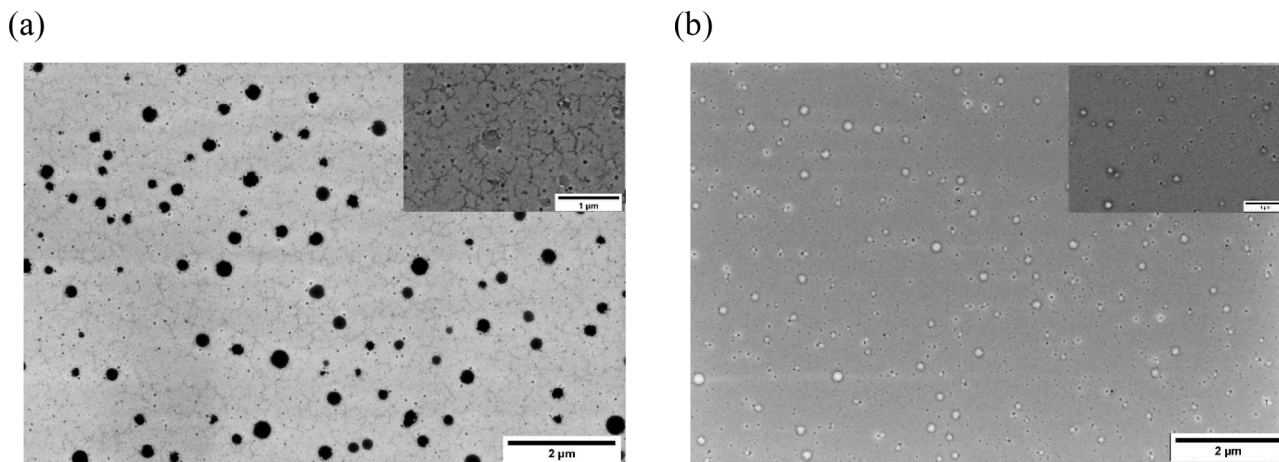
Fig. 5. The plan-view SEM images of nitrogen-doped GeTe samples (a) with 5% nitrogen and (b) 10% nitrogen heated to 450 °C and cooled back to RT. The insets show backscattered electron images at higher magnification showing precipitation of the second phase (excess Ge) at the grain boundaries. Due to the lack of any excess Ge in 10% N doped films such grain boundary precipitation appears to have been avoided.

grain boundaries was completely avoided. As a result, GeTe grains and grain boundaries were indistinguishable in 10% N doped films (Fig. 5b). Another notable observation is that nitrogen doping significantly reduced the number and size of blisters formed at the surface. The samples doped with 10% nitrogen did not show any blisters formation in the capping layer. It is possible that the physical properties of the GeTe films such as elastic modulus and coefficient of thermal expansion and residual stress level changed significantly with the nitrogen doping. However, these aspects are beyond the scope of this paper and will be addressed in future work.

The XRD performed during *in-situ* annealing (5 °C/min) of undoped and nitrogen-doped films agree well with the interpretation from SEM micrographs. Fig. 6 shows XRD patterns of the films as a function of temperature. The undoped films were heated to a maximum temperature of 465 °C while the N-doped films were heated to 600 °C (shown using a horizontal black line in Fig. 6a-c) and then cooled to RT. Initially at RT, no diffraction peaks were visible which confirms that the sample was amorphous in an as-deposited state. The diffraction peaks attributed to the GeTe rhombohedral phase appear when T_x is reached. With further heating, cubic Ge peaks appear at temperature T_{Ge} in undoped and 5% N-doped films. Such Ge peaks were not visible in 10% nitrogen-doped films, which is also consistent with the SEM conclusions. For clarity, the peak profiles of the undoped and N-doped samples after cooling to RT are shown in Fig. 6d.

Fig. 7 shows curvature measurements during the crystallization cycle in undoped and nitrogen doped GeTe films. Consistent with the previous reports on the effect of nitrogen doping on GeTe crystallization the nitrogen-doped samples showed higher crystallization temperature [2,5, 10]. Interestingly, the magnitude of sharp tensile stress build-up at the GeTe crystallization point (T_x) was progressively reduced with the amount of nitrogen doping. Furthermore, consistent with our SEM observations related to lesser grain boundary precipitation of excess Ge in 5%N-doped samples (Fig. 5a), curvature measurements reflected the reduced magnitude of compressive stress jump at T_{Ge}. The films doped
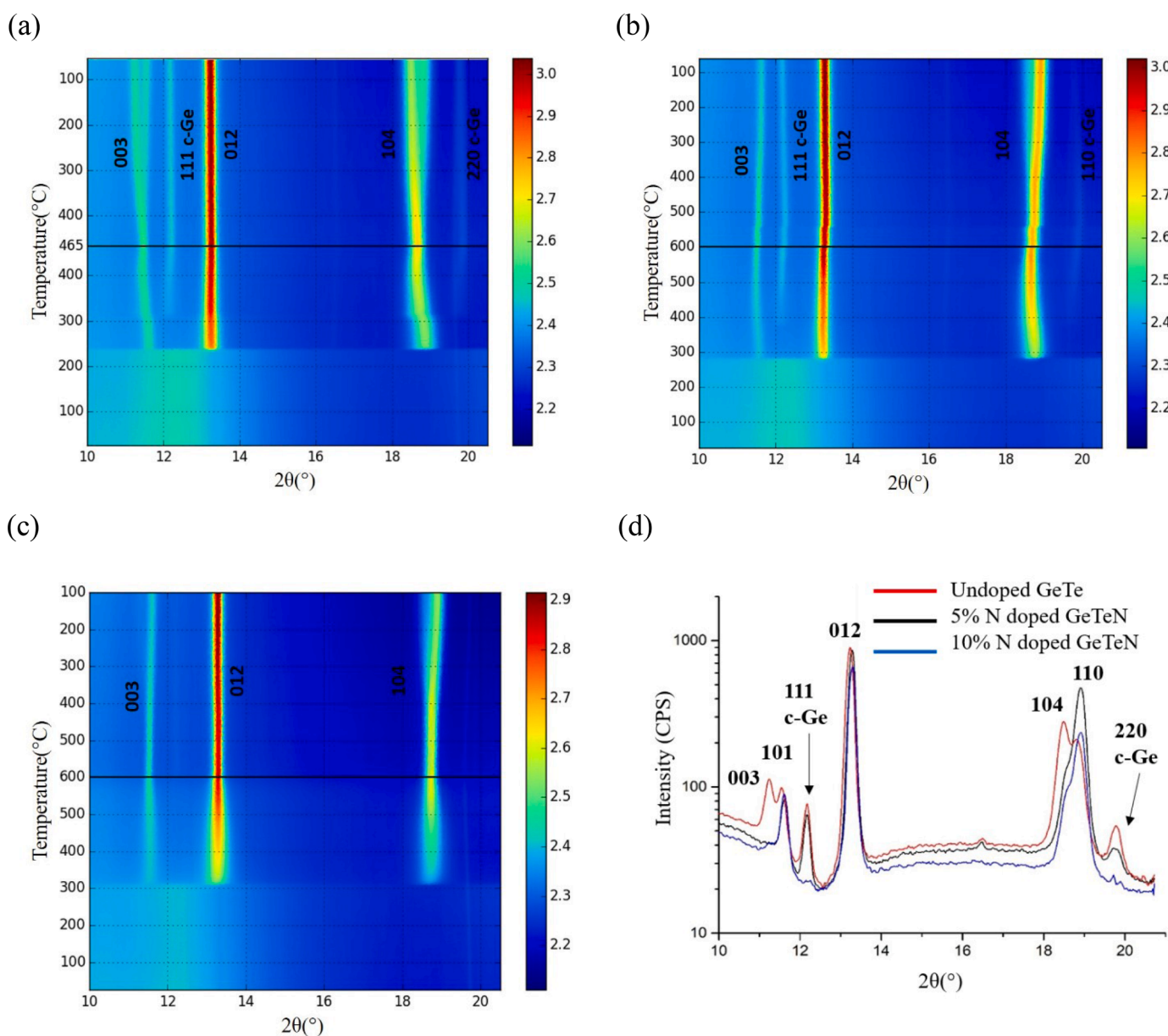

Fig. 6. XRD patterns acquired during *in-situ* annealing of 100 nm (a) GeTe (undoped) (b) 5% N doped GeTe and (c) 10% N doped GeTe films. (d) peak profiles of undoped and doped films after cooling down. No cubic Ge peaks are detected in 10% N doped GeTe film. The intensity of the peaks is shown using a color-coded bar. For interpretation of the reference to color in this figure legend, the reader is referred to the web version of this article.
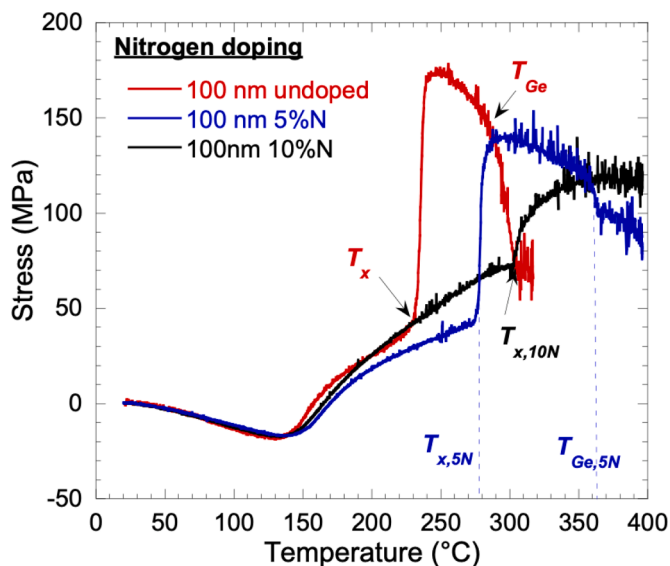
Fig. 7. The stress change in 100 nm undoped and nitrogen-doped GeTe films during heating up to 400 °C. T_x for GeTe crystallization and T_{Ge} for Ge precipitation for different film compositions are shown using arrows and dotted lines. At T_x and T_{Ge} stress changes abruptly in tensile and compressive directions, respectively.

with 10% nitrogen did not show compressive stress build-up at T_{Ge} implying a lack of any Ge precipitation at the grain boundaries (Fig. 5b).

Finally, the crystallization of GeTe was studied under isothermal conditions to understand the kinetics of crystallization process. The samples were heated and held at a constant temperature slightly below the GeTe crystallization temperature and the curvature change was continuously monitored. These measurements are shown in Fig. 8. It was observed that at the lowest temperature the crystallization proceeded rather slowly. The sample did not fully crystallize even after 19 h of annealing. At a slightly higher temperature, the samples were fully crystallized within 19 h annealing and the kinetics of crystallization
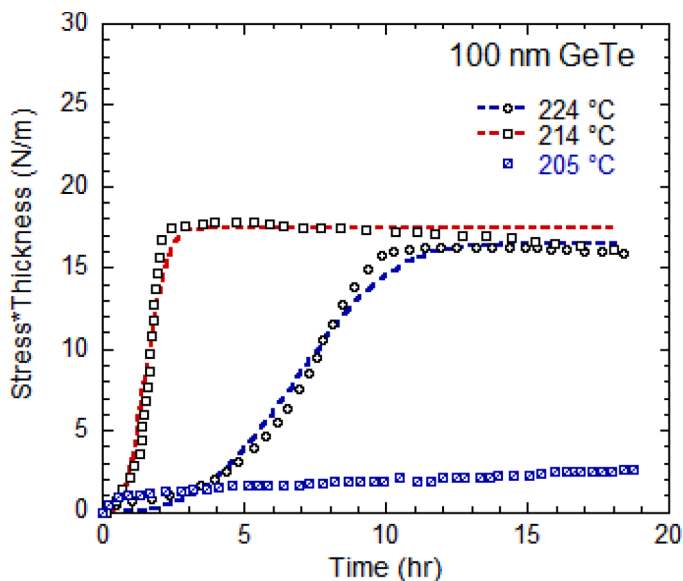

Fig. 8. The curvature change recorded during crystallization of 100 nm GeTe films under isothermal condition at different temperatures indicated in the figure legends. The samples were heated to the final temperature with a 2 °C/min heating rate. The heating stage is omitted and only curvature change after reaching a temperature set point is shown. The data along the ordinate is shifted to begin from zero and fitted with the JMAK model.

become drastically fast with a slight increase in the temperature. The crystallization of GeTe, therefore, occurs over a very narrow temperature range which presents a difficulty in studying the kinetics of GeTe crystallization. The Johnson-Mehl-Avrami-Kolmogorov (JMAK) kinetic model that describes the kinetics of phase transformation (discussed in the next section) reasonably fits the curvature vs. time data shown in Fig. 8.

Similarly, the kinetics of crystallization of excess Ge was studied using isothermal crystallization measurements performed at temperatures slightly below the crystallization temperature of Ge, T_{Ge}. Fig. 9 shows the stress evolution during isothermal Ge crystallization. At temperatures slightly above the T_x the stress remains constant (blue curve in Fig. 9). This suggests that the kinetics of Ge crystallization are extremely sluggish and there is no stress relaxation in the crystallized GeTe and amorphous network of excess Ge present at this temperature. As the temperature is increased close to T_{Ge} excess Ge shows a similar sigmoidal transformation observed during the crystallization of GeTe. However, unlike GeTe crystallization which occurs in the amorphous phase and hence can rapidly relax the volumetric stress due to GeTe crystallization, the excess Ge crystallizes along grain boundaries in GeTe which does not relax the stress so efficiently. This has important implications for observed stress during these two crystallization events and will be discussed in the following section. A fully crystallized sample, wherein, both GeTe and excess Ge has crystallized do not show any appreciable stress relaxation during isothermal annealing (See Supplementary Material Fig. S4).

4. Discussion

The curvature ($\kappa \propto \sigma.h$) measurements during the crystallization cycle showed dynamic changes in film stress from compressive to tensile and back to compressive stress as shown in Fig. 1. The substrate curvature measurements monitor the total stress in the film composed of

$$\sigma_{tot} = \sigma_{int} + \sigma_{th} \qquad (2)$$

where, σ_{int} is the internal stress (due to viscous relaxation, crystallization, precipitation, etc.) and $\sigma_{th} = M_f \Delta \alpha \Delta T$ is the thermal stress imposed due to heating and cooling, where, M_f is the biaxial modulus of the film, $\Delta \alpha$ is the difference in the coefficient of thermal expansion between film and substrate and ΔT is the temperature change. Therefore, real-time monitoring of the curvature changes during the phase transformation provides valuable information about the kinetics of internal stress changes in the films and can shed light on the underlying processes responsible for it. We will first discuss relaxation in the amorphous phase and later address the sharp rise and fall in stress correlated with crystallization of amorphous GeTe and excess Ge respectively.

4.1. Relaxation in the amorphous phase

The sputtering of atoms at a high deposition rate or at low T_{sub}/T_m (T_{sub} is substrate temperature and T_m is melting point of material) resulting in low surface mobility promotes the formation of an amorphous film. Due to frozen-in atomic configurations, dangling bonds, and lack of long-range order; the amorphous structure is far from its thermodynamic equilibrium. EXAFS studies [22,34,37–40] have shown that amorphous GeTe films contain several kinds of defects such as atoms with wrong coordination numbers, stretched or compressed atomic bonds, variation in bond angles, excess vacancies, etc. During isothermal annealing, the amorphous (highly disordered) structure tends to reach lower energy (metastable) state by a series of atomic jumps driven by random density fluctuations. This is commonly known as "structural relaxation" in amorphous solids.

Much of the understanding of structural relaxation in amorphous solids is derived from previous studies on glass-forming materials [54–60] and sputter-deposited amorphous thin films [54,61–64]. A
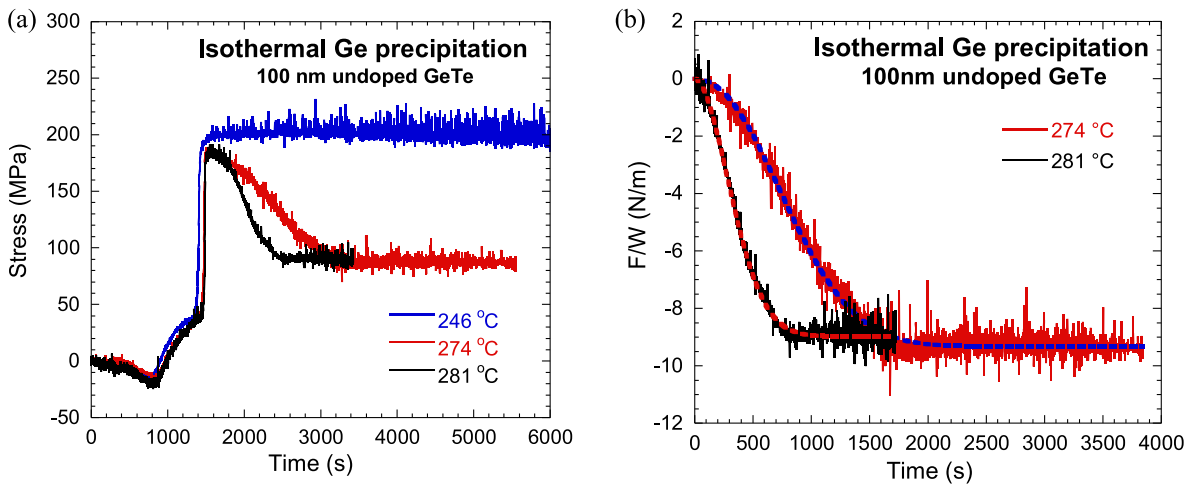
Fig. 9. (a) stress evolution in GeTe thin films during heating from RT to a final temperature indicated in the legend followed by isothermal hold. The initial data to ~1500s is heating stage followed by isothermal holds once the desired set temperatures is reached. (b) Stress × thickness data during isothermal hold after reaching a desired temperature setpoint. The excess Ge crystallization shows a typical sigmoidal transformation. The data along the ordinate is also shifted to begin from zero and fitted with the JMAK model.

time-dependent change in the viscosity was often observed and hence is a characteristic of all amorphous materials. Most of the silicate glasses and melt quenched glasses as well as chalcogenide glasses have shown a linear increase in the viscosity with time given by $\eta(t) = \eta_0 + \dot{\eta}t$ where, η_0 and $\dot{\eta}$ are constants [54,62,65]. It was proposed that the time-dependent viscosity change is a result of structural relaxation during which the excess defects in the amorphous phase are annihilated. Witvrouw and Spaepen [54] modeled such viscous relaxation in amorphous glass films by considering the flow of defect concentration. The model considered decay of defect concentration c during annealing by unimolecular ($dc/dt = -k_1 c$) or bimolecular annihilation processes ($dc/dt = -k_2 c^2$). The change in the defect concentration in the film directly relates to the change in the viscosity as well as stress in the films [54,62,64]. Based on this, the evolution of stress in amorphous thin films was predicted. Previous studies have shown that the bimolecular annihilation model (Eq. (3)) better predicted the stress relaxation in amorphous phases change materials [14,54,61,62] than the unimolecular model.

$$ln\frac{\sigma}{\sigma_0} = -\frac{M_f}{6\dot{\eta}}ln\left(1 + \frac{\dot{\eta}t}{\eta_0}\right) \qquad (3)$$

where, M_f is the biaxial modulus of the film, $\dot{\eta}$ and η_0 are constants related to initial defect density c_0 by a relationship $\dot{\eta} = \eta_0 c_0 k_2$. The bimolecular defect annihilation model, Eq. (3), and its curve-fitting on the stress relaxation observed in the undoped GeTe films at different temperatures (previously shown in Fig. 2a) are re-plotted in Fig. 10a. The model fits the experimental stress relaxation data accurately, consistent with the previous studies [14,61].

The parameters $\dot{\eta}$ and η_0 are obtained from the non-linear least square curve fitting, given in Table 1. The activation energy of 0.27 eV was obtained for the undoped GeTe films from the Arrhenius temperature dependence of kinetic parameter $\dot{\eta}$ (See Fig. 10b). This value is close to the activation energy for self-diffusion in GeTe found through experiments and simulations [66,67].
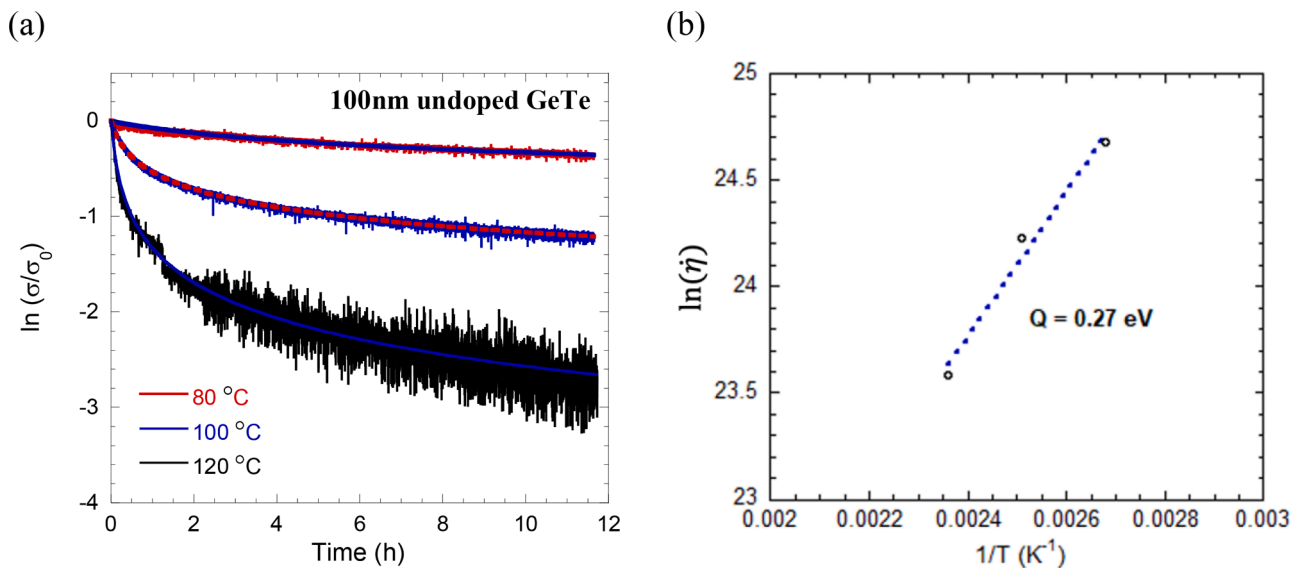
Fig. 10. (a) The stress relaxation data of 100 nm undoped GeTe thin films at different isothermal annealing temperatures fitted with the bimolecular annihilation model (Eq. (3)). (b) Activation energy obtained from the temperature dependence of the parameter $\dot{\eta}$ obtained from fitting in (a).

Table 1
Fitting parameters obtained by fitting Eq. (3) on the experimental relaxation data (Fig. 10(a)) for undoped, 5% N doped, and 10% N doped GeTe films.

Temprature	Undoped GeTe		5% N doped		10% N doped	
	$\dot{\eta}$ (Pa)	η_0 (Pa. s)	$\dot{\eta}$ (Pa)	η_0 (Pa. s)	$\dot{\eta}$ (Pa)	η_0 (Pa. s)
80 °C	5.21×10^{10}	3.91×10^{14}	3.69×10^{10}	6.46×10^{14}	3.46×10^{10}	3.55×10^{14}
100 °C	3.32×10^{10}	2.36×10^{13}	2.54×10^{10}	4.30×10^{13}	2.11×10^{10}	3.72×10^{13}
120 °C	1.75×10^{10}	6.49×10^{12}	0.91×10^{10}	8.94×10^{12}	1.14×10^{10}	2.49×10^{12}

4.2. Mechanism for crystallization events

In the previous study using combined *in-situ* XRD and curvature measurements, a sharp increase and decrease in the stress were correlated with the crystallization of GeTe and excess Ge, respectively [33]. The X-ray reflectivity (XRR) measurements showed 7% increase (decrease) in the density (thickness) [33] upon GeTe crystallization in undoped GeTe films in agreement with literature [2,9]. Assuming such volume change is accommodated by purely elastic behavior, the calculations yield an unrealistically high stress value of 3.4 GPa. It was argued that a significant amount of stress must be relaxed by the viscous flow in the surrounding amorphous phase during the crystallization process. The kinetics of stress change during isothermal crystallization studied in this work provides a few additional insights into the crystallization mechanism of GeTe and can help resolve this discrepancy.

The stress evolution during isothermal crystallization just below T_x, as shown in Fig. 8, showed a typical sigmoidal shape, which is a characteristic of classical nucleation and growth theory. The models for kinetics of phase transformations were developed in the works of Kolmogorov [68], Johnson and Mehl [69], and Avrami [70,71]. The Johnson-Mehl-Avrami-Kolmogorov (JMAK) kinetic model captures the kinetics of most of the isothermal transformations that occur by nucleation and growth such as polymorphic phase changes, recrystallization [72], and solid-state dewetting [73,74].

The basic Avarami model predicts the fraction of the transformed phase by the following equation

$$X^c = 1 - \exp(-kt^n) \tag{4}$$

where k is the rate constant and n is the Avrami time exponent. More physics can be added to the basic model of Avrami to get additional information about the nucleation rate and growth velocity [72]. According to JMAK kinetic model, the crystallized fraction is given as

$$X^c = 1 - \exp\left(-\frac{\pi}{3}u^3t^4I_v\right) \tag{5}$$

The model assumes isotropic growth velocity (u) of the spherical nuclei until they impinge on other growing crystals and random homogeneous nucleation at a constant rate, I_v. If the force per unit width (F/W) varies from F_0 to F_f as the fraction crystallized, X^c, changes from 0 to 1 during crystallization we can write Eq. (5) in terms of film force as

$$F_t = F_f\left[1 - \exp\left(-\frac{\pi}{3}u^3t^4I_v\right)\right] \tag{6}$$

Where, F_t is force per unit width of the film at any time t, F_f is the final value of F/W at the end of GeTe crystallization, I_v is a number of nuclei per unit volume per second, u is the average growth velocity, and the Avrami time exponent $n = 4$. The Avrami exponent $n = 4$ was chosen for the fitting because the fitting procedure predicts a value close to 4 if the parameter n is selected as an adjustable free fitting parameter. The values of growth velocity and nucleation rate remain less affected by the fitting with n as an adjustable parameter (see Table 3). This supports the spherical nucleation assumed in the model (Eqs. (5) and(6)) was used to fit the data obtained from curvature measurement during isothermal

Table 3
The parameters obtained by fitting Eq. (6) to the stress x thickness (F/W) change during crystallization during the isothermal annealing are shown in Fig. 8 with Avrami exponent n as a free and fixed parameter.

| 214 °C			224 °C		
I_v (m^{-3} s^{-1})	u (μm/s)	n	I_v (m^{-3} s^{-1})	u (μm/s)	n
2.13×10^{-6}	67.2	3.7	1.33×10^{-5}	198.1	4.8
1.57×10^{-6}	64.4	4.0	2.25×10^{-5}	192.9	4.0

crystallization shown in Fig. 8. The excellent agreement between data and the JMAK model suggests that the fraction of tensile force developed during GeTe crystallization (F_t/F_f) directly correlates with the fraction of crystallized GeTe phase and the remainder of the amorphous phase is stress-free. The parameters obtained from the curve fitting (Eq. (6)) are given in Table 3. The important parameters i.e., nucleation rate (I_v) and growth velocity (u) extracted from curve fitting suggest that nucleation rate increased by an order of magnitude with a slight 10 °C increase in the temperature. However, the growth speed increased only by a factor of 3. This suggests that GeTe crystallization is a nucleation-controlled process.

Additionally, due to the inherent assumption of grain boundary interface formation upon impingement in the JMAK model; it is necessary to consider the stress originating from the formation of grain boundary interface between the crystallized GeTe grains. Both the crystalline and amorphous phases co-exist during the crystallization process. The stress generated due to volume change when crystalline GeTe nucleates and grow in the amorphous matrix can rapidly relax due to rapid stress relaxation in the surrounding amorphous phase at such high temperatures. Therefore, stress remains low until the growing crystalline nuclei start to impinge on each other. Once the impingement begins stress begins to build up rapidly due to grain boundary formation by grain coalescence process. Once most of the amorphous GeTe phase is transformed into the crystalline GeTe phase the grain boundary formation slows down and stress begins to saturate giving rise to the typical sigmoidal shape of F/W vs time curve shown in Fig. 8. To support the grain coalescence process, it is important to look at the microstructural changes in the GeTe films during the crystallization process, especially the grains structure.

4.2.1. Microstructural changes during crystallization

The sputter-deposited amorphous films often show a porous structure in which atoms are randomly packed in nanofibers consistent with Thornton's structure zone diagrams [75,76]. In previous work, Khoo *et al.* observed nanofibrous structure in sputter-deposited amorphous GeTe with trapped nanovoids [77]. The nanofibrous structure in sputter-deposited amorphous films was also macroscopically modelled [78] and observed during sputter deposition of amorphous Si and Ge films at a temperature higher than RT [79]. Therefore, nanofibrous growth with the random atomic arrangement is common in a variety of sputter-deposited amorphous thin films.

A cross-section of crystallized GeTe film was analyzed using TEM and SEM and is shown in Fig. 11. A cross-section lamella, from the crystallized GeTe sample (heated above T_x and cooled back to RT), was prepared using FIB milling and polishing for TEM analysis. TEM dark field and bright field imaging did not reveal any grain boundary contrast between GeTe grains most likely due to surface oxidation during sample storage in ambient atmosphere inbetween FIB and TEM experiments. However, EDS line profile analysis at the center of the film (Fig. 11a) clearly showed peaks of high (low) atomic concentration of Ge (Te) as shown in Fig. 11b. This is consistent with the dark contrast observed in SEM plan view micrographs that showed a thin shell of lighter atomic species (such as Ge atoms) segregated at the grain boundaries. SEM micrographs taken at the cross-section of the cleaved Si edge, shown in Fig. 11c, clearly show a columnar grain structure in the crystallized GeTe films.

(a)

(b)

(c)
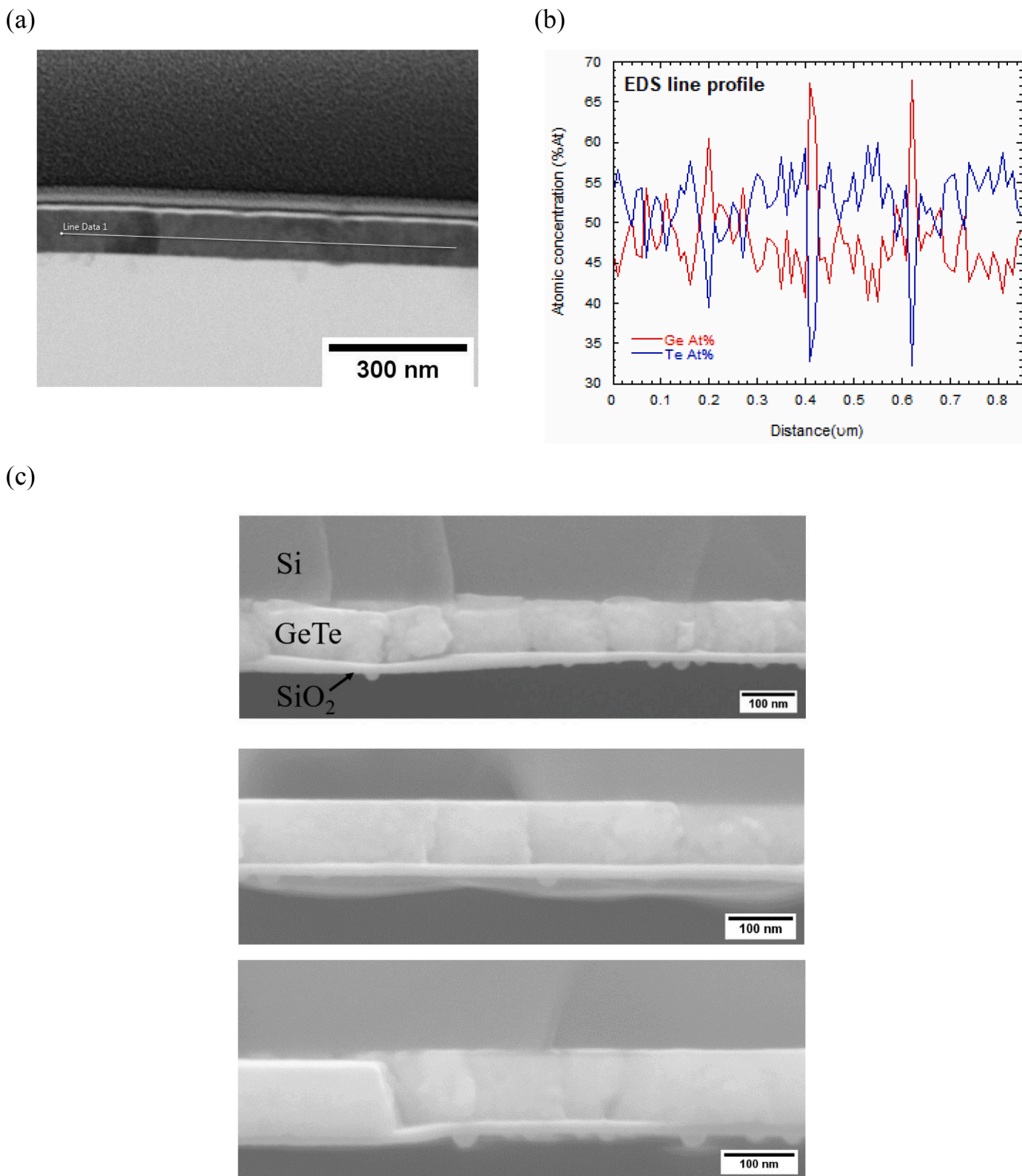
Fig. 11. (a) TEM image of a cross-section lamella prepared using FIB milling and polishing showing the region where EDS line scan was taken (b) corresponding EDS elemental mapping along a line shown in (a). (c) Multiple SEM images of cleaved Si edge showing columnar grains in fractured GeTe film.

4.2.2. Coalescence of GeTe grains during crystallization

The transformation from the amorphous structure to the poly-crystalline columnar GeTe grain structure supports grain coalescence process and is illustrated schematically in Fig. 12. At the crystallization temperature, spherical nuclei nucleate randomly. Since the growth dimensions are much greater than the film thickness, the nuclei quickly grow along the thickness direction and then essentially grow radially in 2-Dimensions until they impinge on other growing crystals in the vicinity. When two crystals impinge on each other they coalesce together and form a grain boundary. In coalescence process, two amorphous-
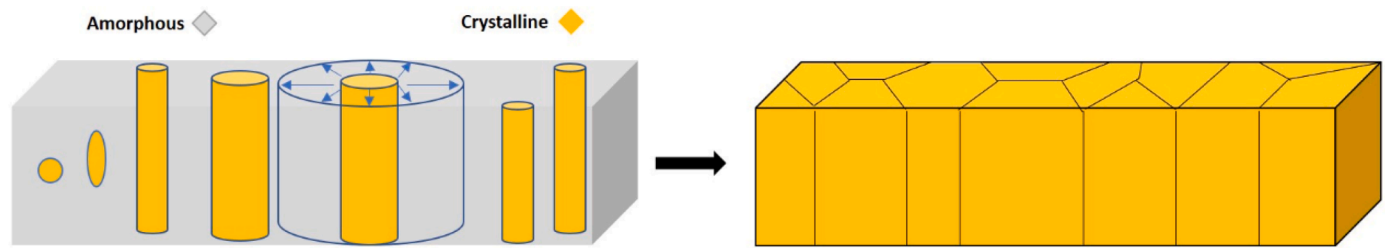
Fig. 12. Schematic showing crystallization process producing columnar polycrystalline GeTe. The rejected Ge is located at the grain boundaries (black lines in the right panel).

crystalline interfaces of adjacent crystals get replaced by a grain boundary. The grain boundary formation is also consistent with the sharp drop in the resistance at a crystallization temperature of GeTe as the grains become connected [36]. The excess Ge is rejected as the GeTe crystals grow and segregate along the grain boundaries forming an amorphous shell of excess Ge surrounding GeTe grains.

During coalescence, individual GeTe crystals are stretched to form a grain boundary. The driving force for the process can be related to the difference between amorphous-crystalline interface (γ_{ac}) and grain boundary (γ_{gb}) energies ($\Delta\gamma = \gamma_{ac} - 1/2\gamma_{gb}$). The mechanism is similar to the one proposed by Hoffman and later by Nix and Clemens [80,81] to model the coalescence of islands during initial stage of thin film growth. Freund and Chason [82] extended and generalized the model so that it can be applied to different contact problems. For the case of coalescence of two cylinders with diameter R and height h the average volume stress can be estimated by the following formula

$$\sigma_{avg} = 0.44 \frac{E^{1/3}\Delta\gamma^{2/3}}{R^{2/3}} \tag{7}$$

where E is the biaxial modulus of the film, $\Delta\gamma = \gamma_{ac} - 1/2\gamma_{gb}$ and R is the grain size. Using a value of elastic modulus of the GeTe films as 43 GPa (determined using double substrate curvature measurements), a typical ballpark value of $\Delta\gamma \sim 1$ J/m^2, and an average grain size of 50 nm; the average stress that is expected by coalescence mechanism (Eq. (7)) was estimated to be 114 MPa which is very close to the experimentally observed stress change of 129 MPa. Therefore, the predictions based on the coalescence model are much closer to experimental observations than the simple volume change-based elastic predictions. We conclude that at variance with the most straightforward interpretation of stress build-up caused by density change [33,43], the stress evolution during GeTe crystallization is caused by crystallite coalescence.

4.2.3. GeTe crystallization in N-doped samples

The crystallization behavior of the N-doped samples further supports the coalescence mechanism. Fig. 7 showed the curvature change during the crystallization of undoped and N-doped GeTe films of the same thickness. It is apparent that the magnitude of tensile stress upon GeTe crystallization progressively reduces with the amount of nitrogen introduced into the films. Additionally, the crystallization is achieved at higher temperatures with N doping consistent with the previous observations [5,25,83]. It is well known that nitrogen atoms preferentially form Ge-N covalent bonds in the process of forming stable GeN$_x$ nitride molecules [5,28,83]. The in-situ synchrotron diffraction study have shown that the presence of Ge-nitride molecules prevents the GeTe crystallization in Ge-rich GST films [50]. In context of coalescence mechanism disscused here, the presence and segregation of nitride molecules in-between GeTe crystallites can make the coalescence process energetically unfeasible by altering the crystalline-amorphous interface and grain boundary energies. Thus, leading to a lesser magnitude of tensile stress during the crystallization of N-doped GeTe films as observed in the experiments. Note that the tensile stress produced by the coalescence model (Eq. (7)) is inversely proportional to the

grain size. If nitrogen doping causes grain refinement in GeTe films then the tensile stress magnitude is expected to increase with increasing nitrogen amount opposite of what was observed in the experiments. Therefore, it can be concluded that nitrogen doping does not lead to significant grain refinement in GeTe films. The effect of doping elements (N, C, O) on the volume change in GeTe and GST films (during crystallization) is also well known [10,24–26,84,85]. However, as mentioned before, the stresses originating from densification/volume change during crystallization overpredict the stress by orders of magnitude. A decrease in GeTe film thickness upon crystallization in lightly nitrogen doped (0.5–1 at% N) samples was observed whereas, in heavily N-doped GeTe films (>4 at% N) an increase in the film thickness was observed in a previous study [10]. Therefore, clearly, volume change does not explain the tensile stress build-up during crystallization of the doped films.

The SEM images of nitrogen-doped samples also showed a reduction in excess Ge precipitation along the grain boundaries with an increasing amount of nitrogen doping (see Fig. 5). Due to more favourable Ge-N bonds, fewer Ge atoms were available for precipitation in 5% N-doped films. The Ge precipitation was not detected in the films doped with 10% N because all Ge atoms are bonded to N in agreement with XRD results that do not show a crystalline Ge peak. This is consistent with the curvature measurement of undoped and doped samples as shown in Fig. 7. The compressive stress induced by excess Ge precipitation at T_{Ge} was significantly reduced with just 5% N doping while it was not observed in samples with 10% N doping. Therefore, the magnitude of compressive stress upon excess Ge precipitation is expected to strongly depend on the stoichiometry of the GeTe composition and excess Ge atoms available for precipitation. This needs to be investigated further using different Ge-rich GeTe compositions.

4.3. Crystallization of excess Ge

The crystallization of excess Ge also showed a sigmoidal shape of stress × thickness vs time curve shown in Fig. 9. The fitting of the basic Avrami model, Eq. (4), on stress × thickness vs time curve predicts an Avrami exponent $n = 2$. The value of $n = 2$ suggests that the nucleation occurs predominantly at the grain corners [72] and growth proceeds along the grain boundary as observed in the SEM micrographs shown in Fig. 4. Therefore, the crystallization of excess Ge is fundamentally different from the crystallization of GeTe and such insights can be obtained simply from the fitting of JMAK model. The growth of crystallized Ge along grain boundaries in GeTe produces a volumetric strain and thus leads to a compressive stress in the surrounding grains.

The density of crystalline diamond cubic Ge is a few percent less than the amorphous Ge [86]. This produces a positive volume change during excess Ge crystallization. Consequently, compressive stress is expected during excess Ge crystallization similar to what was measured by curvature measurements. The prediction of the magnitude of compressive stress build-up during excess Ge crystallization, however, remains challenging. A previous study [33] showed a 1.5% increase in the unit cell volume in GeTe at T_{Ge}. But again, purely elastic calculations with 1.5% volume change predict order of magnitude higher compressive

stress compared with the curvature measurements that recorded a compressive stress build-up of approximately 84 MPa in 100 nm GeTe films. The Ge precipitation-induced stress also depends on the amount of excess Ge atoms available for precipitation as seen in N-doped GeTe samples. Therefore, the magnitude of compressive stress during Ge crystallization is very sensitive to GeTe alloy composition i.e., excess Ge in the alloy. Further experiments with different stoichiometric compositions of Ge-rich GeTe films and TEM analysis of grain boundaries (before and after Ge precipitation) will be useful to develop a more quantitative model for the compressive stress build-up related to excess Ge precipitation along the grain boundaries. The precipitation of excess Ge in the form of separate Ge grains within the GeSbTe matrix was also observed in some of the previous work on GST films [87]. We found Ge precipitation occurred predominantly along GeTe grain boundaries. However, this scenario can change in highly Ge-rich compositions of GeTe.

To summarize, based on the curvature measurements on undoped and nitrogen-doped GeTe thin films, the amorphous to polycrystalline transition can be divided into the three distinct stages (i) structural rearrangement/relaxation of as-deposited amorphous structure at $T < T_x$ (ii) at T_x nucleation and growth of GeTe crystals occur until they impinge on each other. This is followed by the coalescence of individual crystals forming grain boundaries leading to a tensile stress jump. The excess Ge is rejected during the growth of GeTe crystals, and it forms a shell of amorphous Ge along certain GeTe grain boundaries (iii) at T_{Ge} the excess Ge precipitates along GeTe grain boundaries leading to compressive stress in the films.

5. Conclusions

Curvature measurements during phase transformation in undoped as well as nitrogen-doped GeTe films were used to gain insights into the physical processes at work during the phase transitions. The structural relaxation in the amorphous phase was observed during annealing below the crystallization temperature. The densification of the amorphous film occurred during stress relaxation accompanied by the rearrangement of atoms leading to a change in the viscosity of the amorphous film. The stress relaxation in amorphous phase can be accurately predicted by a bimolecular defect annihilation model. The isothermal crystallization indicated that the transformation was governed by nucleation and growth phenomenon. At crystallization temperature individual nanocolumnar GeTe crystals grew and coalesced together upon impinging on each other; in the process forming grain boundaries and led to polycrystalline GeTe. In this process, a tensile stress build-up was observed as a result of grain coalescence. Excess Ge is rejected by growing GeTe crystals segregated along GeTe grain boundaries forming a network-like structure of amorphous Ge. At higher temperatures, excess Ge atoms precipitated along the grain boundaries of GeTe grains. Nitrogen doping significantly changed the crystallization behavior of GeTe films. The amount of nitrogen doping progressively (i) increased the crystallization temperature (ii) reduced the magnitude of crystallization-induced tensile stress and (iii) reduced the magnitude of compressive stress due to excess Ge precipitation along the grain boundaries. At higher nitrogen doping concentrations all excess Ge atoms preferentially formed GeN_x and Ge precipitation was completely prevented. It is worth emphasizing that this work resolves the disagreement between the measured stress build-up upon crystallization and the predicted stress value based on the density change upon crystallization.

Declaration of Competing Interest

The authors declare that they have no known competing financial interests or personal relationships that could have appeared to influence the work reported in this paper.

Acknowledgement

Supplementary materials

Supplementary material associated with this article can be found, in the online version, at doi:10.1016/j.mtla.2023.101738.

References

[1] D. Lencer, M. Salinga, B. Grabowski, T. Hickel, J. Neugebauer, M. Wuttig, A map for phase-change materials, Nat. Mater. 7 (2008) 972–977, https://doi.org/10.1038/NMAT2330.

[2] P. Noé, C. Vallée, F. Hippert, F. Fillot, J.Y. Raty, Phase-change materials for non-volatile memory devices: from technological challenges to materials science issues, Semicond. Sci. Technol. 33 (2018), 013002, https://doi.org/10.1088/1361-6641/AA7C25.

[3] G. Bruns, P. Merkelbach, C. Schlockermann, M. Salinga, M. Wuttig, T.D. Happ, J. B. Philipp, M. Kund, Nanosecond switching in GeTe phase change memory cells, Appl. Phys. Lett. 95 (2009), https://doi.org/10.1063/1.3191670.

[4] M. Hase, P. Fons, K. Mitrofanov, A.V. Kolobov, J. Tominaga, Femtosecond structural transformation of phase-change materials far from equilibrium monitored by coherent phonons, Nat. Commun. 6 (2015) 1–6, https://doi.org/10.1038/ncomms9367.

[5] P. Noé, F. Hippert, Structure and properties of chalcogenide materials for PCM. Phase Change Memory devices Physics, Reliability. Applied., Springer, Cham, 2017, pp. 125–179, https://doi.org/10.1007/978-3-319-69053-7_6.

[6] P. Noé, B.J. Kooi, M. Wuttig, Phase-Change and Ovonic Materials (Second Edition), in: 15, 2021, 2100078, https://doi.org/10.1002/PSSR.202100078.

[7] M. Wuttig, N. Yamada, Phase-change materials for rewriteable data storage, Nat. Mater. 6 (2007) 824–832, https://doi.org/10.1038/NMAT2009.

[8] A. Redaelli, Phase Change Memory, Springer International Publishing, Cham, 2018, https://doi.org/10.1007/978-3-319-69053-7.

[9] S. Raoux, M. Wuttig, Phase Change Materials: Science and Applications, Springer Science & Business Media, 2008, https://doi.org/10.1007/978-0-387-84874-7.

[10] Y. Yin, H. Zhang, S. Hosaka, Y. Liu, Q. Yu, Volume-change-free GeTeN films for high-performance phase-change memory, J. Phys. D Appl. Phys. 46 (2013), 505311, https://doi.org/10.1088/0022-3727/46/50/505311.

[11] K. Do, D. Lee, D.H. Ko, H. Sohn, M.H. Cho, TEM study on volume changes and void formation in Ge2Sb 2Te5 films, with repeated phase changes, Electrochem. Solid State Lett. 13 (2010) H284, https://doi.org/10.1149/1.3439647/XML.

[12] D. Ielmini, Drift phenomena in phase change memories, in: World Scientific Reference of Amorphous Materials, The: Structure, Properties, Modeling and Main Applications, 3, World Scientific Publishing Co., 2020, pp. 341–365, https://doi.org/10.1142/9789811215575_0011. Vol.

[13] M.L. Gallo, D. Krebs, F. Zipoli, M. Salinga, A. Sebastian, Collective structural relaxation in phase-change memory devices, Adv. Electron. Mater. (2018) 4, https://doi.org/10.1002/AELM.201700627.

[14] J.Y. Cho, T.Y. Yang, Y.J. Park, Y.C. Joo, Study on the resistance drift in amorphous Ge 2Sb 2Te 5 according to defect annihilation and stress relaxation, Electrochem. Solid State Lett. 15 (2012), https://doi.org/10.1149/2.001204ESL/META.

[15] P. Fantini, M. Ferro, A. Calderoni, S. Brazzelli, Disorder enhancement due to structural relaxation in amorphous Ge 2Sb 2Te 5, Appl. Phys. Lett. (2012) 100, https://doi.org/10.1063/1.4720182.

[16] M. Wimmer, M. Kaes, C. Dellen, M. Salinga, Role of activation energy in resistance drift of amorphous phase change materials, Front. Phys. 2 (2014) 1–12, https://doi.org/10.3389/fphy.2014.00075.

[17] D. Ielmini, S. Lavizzari, D. Sharma, A.L. Lacaita, Temperature acceleration of structural relaxation in amorphous Ge 2 Sb2 Te5, Appl. Phys. Lett. (2008) 92, https://doi.org/10.1063/1.2930680.

[18] M. Mitra, Y. Jung, D.S. Gianola, R. Agarwal, Extremely low drift of resistance and threshold voltage in amorphous phase change nanowire devices, Appl. Phys. Lett. (2010) 96, https://doi.org/10.1063/1.3447941.

[19] M. Rizzi, A. Spessot, P. Fantini, D. Ielmini, Role of mechanical stress in the resistance drift of Ge2Sb 2Te5 films and phase change memories, Appl. Phys. Lett. (2011) 99, https://doi.org/10.1063/1.3664631.

[20] D. Ielmini, M. Boniardi, A.L. Lacaita, A. Redaelli, A. Pirovano, Unified mechanisms for structural relaxation and crystallization in phase-change memory devices, Microelectron. Eng. 86 (2009) 1942–1945, https://doi.org/10.1016/J.MEE.2009.03.085.

[21] P. Noé, C. Sabbione, N. Castellani, G. Veux, G. Navarro, V. Sousa, F. Hippert, F. D'Acapito, Structural change with the resistance drift phenomenon in amorphous GeTe phase change materials' thin films, J. Phys. D Appl. Phys. 49 (2015), 035305, https://doi.org/10.1088/0022-3727/49/3/035305.

[22] J.Y. Raty, W. Zhang, J. Luckas, C. Chen, R. Mazzarello, C. Bichara, M. Wuttig, Aging mechanisms in amorphous phase-change materials, Nat. Commun. 61 (6) (2015) 1–8, https://doi.org/10.1038/ncomms8467, 2015.

[23] G. Navarro, V. Sousa, A. Persico, N. Pashkov, A. Toffoli, J.C. Bastien, L. Perniola, S. Maitrejean, A. Roule, P. Zuliani, R. Annunziata, B. De Salvo, Material engineering of GexTe100−x compounds to improve phase-change memory performances, Solid. State. Electron. 89 (2013) 93–100, https://doi.org/10.1016/J.SSE.2013.07.005.

[24] X. Zhou, W. Dong, H. Zhang, R.E. Simpson, A zero density change phase change memory material: GeTe-O structural characteristics upon crystallisation, Sci. Rep. 5 (2015), https://doi.org/10.1038/srep11150.

[25] M. Putero, M.V. Coulet, C. Muller, C. Baehtz, S. Raoux, H.Y. Cheng, Ge-doped GaSb thin films with zero mass density change upon crystallization for applications in phase change memories, Appl. Phys. Lett. 108 (2016), 101909, https://doi.org/10.1063/1.4943788.

[26] Z. Xu, B. Liu, Y. Chen, D. Gao, H. Wang, Y. Xia, Z. Song, C. Wang, N. Zhu, J. Ren, Y. Zhan, The suppressing of density change in nitrogen doped Ge2Sb2Te5 for high performance phase change memory, ECS Solid State Lett. 4 (2015) P105–P108, https://doi.org/10.1149/2.0121512ssl.

[27] J. Orava, D.W. Hewak, A.L. Greer, Fragile-to-strong crossover in supercooled liquid Ag-In-Sb-Te Studied by ultrafast calorimetry, Adv. Funct. Mater. 25 (2015) 4851–4858, https://doi.org/10.1002/adfm.201501607.

[28] J.Y. Raty, P. Noé, G. Ghezzi, S. Maîtrejean, C. Bichara, F. Hippert, Vibrational properties and stabilization mechanism of the amorphous phase of doped GeTe, Phys. Rev. B Condens. Matter Mater. Phys. 88 (2013) 14203, https://doi.org/10.1103/PhysRevB.88.014203.

[29] E. Huber, E.E. Marinero, Laser-induced crystallization of amorphous GeTe: a time-resolved study, Phys. Rev. B 36 (1987) 1595–1604, https://doi.org/10.1103/PHYSREVB.36.1595.

[30] N. Yamada, E. Ohno, K. Nishiuchi, N. Akahira, Rapid - phase transitions of GeTe -Sb 2 Te 3 pseudobinary amorphous thin films for an optical disk memory, J. Appl. Phys. 69 (1991) 223, https://doi.org/10.1063/1.348620.

[31] X. Sun, E. Thelander, P. Lorenz, J.W. Gerlach, U. Decker, B. Rauschenbach, Nanosecond laser-induced phase transitions in pulsed laser deposition-deposited GeTe films, J. Appl. Phys. 116 (2014), 133501, https://doi.org/10.1063/1.4896879.

[32] T. Ouled-Khachroum, M.I. Richard, P. Noé, C. Guichet, C. Mocuta, C. Sabbione, F. Hippert, O. Thomas, Stress buildup during crystallization of thin chalcogenide films for memory applications: in situ combination of synchrotron X-Ray diffraction and wafer curvature measurements, Thin Solid Films 617 (2016) 44–47, https://doi.org/10.1016/J.TSF.2016.02.020.

[33] M. Gallard, M.S. Amara, M. Putero, N. Burle, C. Guichet, S. Escoubas, M.I. Richard, C. Mocuta, R.R. Chahine, M. Bernard, P. Kowalczyk, P. Noé, O. Thomas, New insights into thermomechanical behavior of GeTe thin films during crystallization, Acta Mater. 191 (2020) 60–69, https://doi.org/10.1016/J.ACTAMAT.2020.04.001.

[34] P. Fons, T. Matsunaga, A.V. Kolobov, M. Krbal, J. Tominaga, N. Yamada, Disorder in order: a study of local and global order in Ge-rich Ge-Sb-Te alloys, Phys. Status Solidi Basic Res. 249 (2012) 1919–1924, https://doi.org/10.1002/pssb.201200497.

[35] J. Akola, R.O. Jones, Structural phase transitions on the nanoscale: the crucial pattern in the phase-change materials Ge2 Sb2 Te5 and GeTe, Phys. Rev. B Condens. Matter Mater. Phys. 76 (2007), https://doi.org/10.1103/PhysRevB.76.235201.

[36] V.L. Deringer, W. Zhang, M. Lumeij, S. Maintz, M. Wuttig, R. Mazzarello, R. Dronskowski, Bonding nature of local structural motifs in amorphous GeTe, Wiley Online Libr. 53 (2014) 10817–10820, https://doi.org/10.1002/anie.201404223.

[37] R. Mazzarello, S. Caravati, S. Angioletti-Uberti, M. Bernasconi, M. Parrinello, Signature of tetrahedral Ge in the Raman spectrum of amorphous phase-change materials, APS 104 (2009), https://doi.org/10.1103/PhysRevLett.104.085503.

[38] J.Y. Raty, C. Otjacques, J.P. Gaspard, C. Bichara, Amorphous structure and electronic properties of the Ge1Sb2Te4 phase change material, Solid State Sci. 12 (2010) 193–198, https://doi.org/10.1016/J.SOLIDSTATESCIENCES.2009.06.018.

[39] S. Caravati, M. Bernasconi, T.D. Kühne, M. Krack, M. Parrinello, Coexistence of tetrahedral- and octahedral-like sites in amorphous phase change materials, Appl. Phys. Lett. 91 (2007), https://doi.org/10.1063/1.2801626.

[40] M. Micoulaut, A. Kachmar, T. Charpentier, Tetrahedral germanium in amorphous phase change materials: exploring the isochemical scenario, Phys. Status Solidi Basic Res. 249 (2012) 1890–1896, https://doi.org/10.1002/PSSB.201200398.

[41] E. Chason, P.R. Guduru, Tutorial: understanding residual stress in polycrystalline thin films through real-time measurements and physical models, J. Appl. Phys. 119 (2016), 191101, https://doi.org/10.1063/1.4949263.

[42] B.B. Yahia, M.S. Amara, M. Gallard, N. Burle, S. Escoubas, C. Guichet, M. Putero, C. Mocuta, M.I. Richard, R. Chahine, C. Sabbione, M. Bernard, L. Fellouh, P. Noé, O. Thomas, In situ monitoring of stress change in GeTe thin films during thermal annealing and crystallization, Micro Nano Eng. 1 (2018) 63–67, https://doi.org/10.1016/j.mne.2018.10.001.

[43] T.P.L. Pedersen, J. Kalb, W.K. Njoroge, D. Wamwangi, M. Wuttig, F. Spaepen, Mechanical stresses upon crystallization in phase change materials, Appl. Phys. Lett. 79 (2001) 3597–3599, https://doi.org/10.1063/1.1415419.

[44] R. Tholapi, M. Gallard, N. Burle, C. Guichet, S. Escoubas, M. Putero, C. Mocuta, M.-.I. Richard, R. Chahine, C. Sabbione, M. Bernard, L. Fellouh, P. Noé, O. Thomas, Stress buildup upon crystallization of GeTe thin films: curvature measurements and modeling, Nanomaterials (2020), https://doi.org/10.3390/nano10061247.

[45] A.N.D. Kolb, N. Bernier, E. Robin, A. Benayad, J.L. Rouvière, C. Sabbione, F. Hippert, N. Poe, Understanding the crystallization behavior of surface-oxidized GeTe Thin films for phase-change memory application, ACS Appl. Electron. Mater. 1 (2019) 701–710, https://doi.org/10.1021/ACSAELM.9B00070/SUPPL_FILE/EL9B00070_SI_001.PDF.

[46] S. Basolo, J.F. Bérar, N. Boudet, P. Breugnon, B. Caillot, J.C. Clemens, P. Delpierre, B. Dinkespiler, I. Koudobine, C. Meessen, M. Menouni, C. Mouget, P. Pangaud, R. Potheau, E. Vigeolas, XPAD: pixel detector for material sciences, IEEE Trans. Nucl. Sci. 52 (2005) 1994–1998, https://doi.org/10.1109/TNS.2005.856818.

[47] P. Pangaud, S. Basolo, N. Boudet, J.F. Berar, B. Chantepie, J.C. Clemens, P. Delpierre, B. Dinkespiler, K. Medjoubi, S. Hustache, M. Menouni, C. Morel, XPAD3-S: a fast hybrid pixel readout chip for X-ray synchrotron facilities, Nucl. Instruments Methods Phys. Res. Sect. A Accel. Spectrometers, Detect. Assoc. Equip. 591 (2008) 159–162, https://doi.org/10.1016/j.nima.2008.03.047.

[48] C.L. Bourlot, P. Landois, S. Djaziri, P.O. Renault, E.le Bourhis, P. Goudeau, M. Pinault, M. Mayne-Lhermite, B. Bacroix, D. Faurie, O. Castelnau, P. Launois, S. Rouzire, Synchrotron X-ray diffraction experiments with a prototype hybrid pixel detector, J. Appl. Crystallogr. 45 (2012) 38–47, https://doi.org/10.1107/S0021889811049107.

[49] C. Mocuta, M.I. Richard, J. Fouet, S. Stanescu, A. Barbier, C. Guichet, O. Thomas, S. Hustache, A.V. Zozulya, D. Thiaudière, Fast pole figure acquisition using area detectors at the DiffAbs beamline-synchrotron SOLEIL, J. Appl. Crystallogr. 46 (2013) 1842–1853, https://doi.org/10.1107/S0021889813027453.

[50] O. Thomas, C. Mocuta, M. Putero, M.I. Richard, P. Boivin, F. Arnaud, Crystallization behavior of N -doped Ge-rich GST thin films and nanostructures: an in-situ synchrotron X-ray diffraction study, Microelectron. Eng. (2021) 244–246, https://doi.org/10.1016/J.MEE.2021.111573.

[51] L. Krusin-Elbaum, C. Cabral Jr., K.N. Chen, M. Copel, D.W. Abraham, K.B. Reuter, S.M. Rossnagel, J. Bruley, V.R. Deline, Evidence for segregation of Te in Ge2Sb2Te5 films: effect on the "phase-change" stress, Appl. Phys. Lett. 90 (2007), 141902, https://doi.org/10.1063/1.2719148.

[52] S. Tripathi, P. Kotula, M.K. Singh, C. Ghosh, G. Bakan, H. Silva, C.B. Carter, Role of oxygen on chemical segregation in uncapped Ge2Sb2Te5 thin films on silicon nitride, ECS J. Solid State Sci. Technol. 9 (2020), 054007, https://doi.org/10.1149/2162-8777/AB9A19.

[53] S. Tripathi, P. Kotula, M. Singh, C. Ghosh, G. Bakan, H. Silva, B. Carter, Chemical segregation in Ge2Sb2Te5 thin films during in-situ heating, (2020). https://arxiv.org/abs/2001.08100v1 (accessed November 19, 2021).

[54] A. Witvrouw, F. Spaepen, Viscosity and elastic constants of amorphous Si and Ge, J. Appl. Phys. 74 (1993) 7154–7161, https://doi.org/10.1063/1.355031.

[55] G.W. Scherer, Relaxation in Glass and Composites, Krieger Publishing Co., 1986.

[56] S. Roorda, W.C. Sinke, J.M. Poate, D.C. Jacobson, S. Dierker, B.S. Dennis, D. J. Eaglesham, F. Spaepen, P. Fuoss, Structural relaxation and defect annihilation in pure amorphous silicon, Phys. Rev. B 44 (1991) 3702, https://doi.org/10.1103/PhysRevB.44.3702.

[57] C.A. Volkert, F. Spaepen, Viscosity and structural relaxation in Pd40Ni40P19Si1, Mater. Sci. Eng. 97 (1988) 449–452, https://doi.org/10.1016/0025-5416(88)90091-2.

[58] K.F. Kelton, F. Spaepen, Kinetics of structural relaxation in several metallic glasses observed by changes in electrical resistivity, Phys. Rev. B 30 (1984) 5516, https://doi.org/10.1103/PhysRevB.30.5516.

[59] A.L. Greer, F. Spaepen, Creep, diffusion, and structural relaxation in metallic glasses, Ann. N. Y. Acad. Sci. 371 (1981) 218–237, https://doi.org/10.1111/j.1749-6632.1981.tb55663.x.

[60] A.I. Taub, F. Spaepen, The kinetics of structural relaxation of a metallic glass, Acta Metall. 28 (1980) 1781–1788, https://doi.org/10.1016/0001-6160(80)90031-0.

[61] J. Kalb, F. Spaepen, T.P.L. Pedersen, Viscosity and elastic constants of thin films of amorphous Te alloys used for optical data storage, J. Appl. Phys. 94 (2003) 4908, https://doi.org/10.1063/1.1610775.

[62] A. Witvrouw, P. Campos, F. Spaepen, Elastic constants and viscosity of amorphous PdSi/PdSiFe multilayers, MRS Proc. 239 (1991) 121, https://doi.org/10.1557/proc-239-121.

[63] A. Witvrouw, F. Spaepen, Determination of elastic constants and viscosity of amorphous thin films from substrate curvature, MRS Proc. 188 (1990) 147, https://doi.org/10.1557/proc-188-147.

[64] Y. Ishii, C.S. Madi, M.J. Aziz, E. Chason, Stress evolution in Si during low-energy ion bombardment, J. Mater. Res. 29 (2014) 2942–2948, https://doi.org/10.1557/JMR.2014.350.

[65] A. Witvrouw, F. Spaepen, Determination of the plane stress elastic constants of thin films from substrate curvature measurements: applications to amorphous metals, J. Appl. Phys. 73 (1993) 7344–7350, https://doi.org/10.1063/1.354025.

[66] G.C. Sosso, G. Miceli, S. Caravati, F. Giberti, J. Behler, M. Bernasconi, Fast crystallization of the phase change compound GeTe by large-scale molecular dynamics simulations, J. Phys. Chem. Lett. 4 (2013) 4241–4246, https://doi.org/10.1021/JZ402268V/SUPPL_FILE/JZ402268V_SI_003.AVI.

[67] G.C. Sosso, J. Behler, M. Bernasconi, Breakdown of Stokes–Einstein relation in the supercooled liquid state of phase change materials, Phys. Status Solidi. 249 (2012) 1880–1885, https://doi.org/10.1002/PSSB.201200355.

[68] A.N. kolmogorov, On the statistical theory of the crystallization of metals, Bull. Acad. Sci. USSR Math. Ser. (1937) 355–359.

[69] W.A. Johnson, R.F. Mehl, Reaction kinetics in processes of nucleation and growth, Trans. AIME 135 (1939) 416.

[70] M. Avrami, Kinetics of phase change. i general theory, J. Chem. Phys. 7 (2004) 1103, https://doi.org/10.1063/1.1750380.

[71] M. Avrami, Kinetics of phase change. ii transformation-time relations for random distribution of nuclei, J. Chem. Phys. 8 (2004) 212, https://doi.org/10.1063/1.1750631.

[72] J. Christian, The theory of transformations in metals and alloys. I. Equilibrium and general kinetic theory, 1975. https://pascal-francis.inist.fr/vibad/index.php?action=getRecordDetail&idt=PASCAL7674006072 (accessed April 13, 2020).

[73] E. Jiran, C.V. Thompson, Capillary instabilities in thin, continuous films, Thin Solid Films 208 (1992) 23–28, https://doi.org/10.1016/0040-6090(92)90941-4.

[74] D. Sonawane, A. Choudhury, P. Kumar, New insights into dewetting of Cu thin films deposited on Si, Langmuir 36 (2020) 5534–5545, https://doi.org/10.1021/ACS.LANGMUIR.0C00575/SUPPL_FILE/LA0C00575_SI_004.MP4.

[75] J.A. Thornton, Structure-zone models of thin films, Model. Opt. Thin Film SPIE (1988) 95, https://doi.org/10.1117/12.941846.

[76] J.A. Thornton, High rate thick film growth, Annu. Rev. Mater. Sci. 7 (1977) 239–260, https://doi.org/10.1146/annurev.ms.07.080177.001323.

[77] C.Y. Khoo, H. Liu, W.A. Sasangka, R.I. Made, N. Tamura, M. Kunz, A.S. Budiman, C.L. Gan, C.V. Thompson, Impact of deposition conditions on the crystallization kinetics of amorphous GeTe films, J. Mater. Sci. 51 (2016) 1864–1872, https://doi.org/10.1007/s10853-015-9493-z.

[78] G.S. Bales, A. Zangwill, Macroscopic model for columnar growth of amorphous films by sputter deposition, J. Vac. Sci. Technol. A Vac. Surfaces Film. 9 (1998) 145, https://doi.org/10.1116/1.577116.

[79] J.A. Floro, P.G. Kotula, S.C. Seel, D.J. Srolovitz, Origins of growth stresses in amorphous semiconductor thin films, Phy. Rev. Lett. 91 (2003), 096101, https://doi.org/10.1103/PhysRevLett.91.096101.

[80] R.W. Hoffman, Stresses in thin films: the relevance of grain boundaries and impurities, Thin Solid Films 34 (1976) 185–190, https://doi.org/10.1016/0040-6090(76)90453-3.

[81] W.D. Nix, B.M. Clemens, Crystallite coalescence: a mechanism for intrinsic tensile stresses in thin films, J. Mater. Res. 14 (1999) 3467–3473, https://doi.org/10.1557/JMR.1999.0468.

[82] L.B. Freund, E. Chason, Model for stress generated upon contact of neighboring islands on the surface of a substrate, J. Appl. Phys. 89 (2001) 4866, https://doi.org/10.1063/1.1359437.

[83] A.V. Kolobov, P. Fons, B. Hyot, B. André, J. Tominaga, Y. Tamenori, H. Yoshikawa, K. Kobayashi, Local structure of nitrogen in N-doped amorphous and crystalline GeTe, Appl. Phys. Lett. 100 (2012) 61910, https://doi.org/10.1063/1.3683522.

[84] W. Zhou, L. Wu, X. Zhou, F. Rao, Z. Song, D. Yao, W. Yin, S. Song, B. Liu, B. Qian, S. Feng, High thermal stability and low density variation of carbon-doped Ge2Sb2Te5 for phase-change memory application, Appl. Phys. Lett. 105 (2014), 243113, https://doi.org/10.1063/1.4904832.

[85] M. Xu, Y. Guo, Z. Yu, K. Xu, C. Chen, H. Tong, X. Cheng, M. Xu, S. Wang, C.Z. Wang, K.M. Ho, X. Miao, Understanding CrGeTe3: an abnormal phase change material with inverse resistance and density contrast, J. Mater. Chem. C 7 (2019) 9025–9030, https://doi.org/10.1039/c9tc02963j.

[86] T.B. Light, Density of "amorphous" Ge, Phys. Rev. Lett. 22 (1969) 999, https://doi.org/10.1103/PhysRevLett.22.999.

[87] S.M.S. Privitera, V. Sousa, C. Bongiorno, G. Navarro, C. Sabbione, E. Carria, E. Rimini, Atomic diffusion in laser irradiated Ge rich GeSbTe thin films for phase change memory applications, J. Phys. D Appl. Phys. 51 (2018), 145103, https://doi.org/10.1088/1361-6463/AAB1D0.